Journal of Solid State Chemistry **159,** 10–18 (2001)
doi:10.1006/jssc.2001.9115, available online at http://www.idealibrary.com on IDEAL®

Molecular Dynamics Studies of the Kinetics of Phase Changes in Clusters: Crystal Nucleation of $(RbCl)_{108}$ Clusters at 600, 550, and 500 K

Haishan Deng

Department of Chemistry, Nanjing Normal University, P. R. China

and

Jinfan Huang[1]

Department of Chemistry, University of Michigan, Ann Arbor, Michigan 48109

Received August 24, 2000; in revised form January 10, 2001; accepted February 9, 2001; published online May 4, 2001

Molecular dynamics computer simulations based on the Born–Mayer–Huggins potential function have been employed to study the crystal nucleation of $(RbCl)_{108}$ clusters. When a completely melted $(RbCl)_{108}$ cluster was cooled down at a cooling rate of 2.5×10^{11} K/s, nucleation and crystal growth into the NaCl-type structure crystal was observed at the temperature $\sim$600 K. When a melted $(RbCl)_{108}$ cluster was quenched from 900 K to a bath with a temperature from 600 to 500 K and kept in the bath for a time period up to $\sim$720 ps, both nucleation and crystal growth into the NaCl-type crystals were observed. Nucleation rates of crystallization at 600, 550, and 500 K are estimated and the interfacial free energy of the liquid–solid boundary was derived from the nucleation rates using the classical nucleation theory. The diffuse interface thickness was also estimated. The possibility of the transition from NaCl-type to CsCl-type structure under high Laplace pressure is discussed.

Key Words: **rubidium chloride; crystal nucleation rate; interfacial free energy.**

INTRODUCTION

After Slater discovered the polymorphism in RbBr and RbI at high pressure (1), Jacobs found the structure of high-pressure form of RbI is CsCl type (2). Some other alkali halides such as RbCl, KCl, KBr, and KI were also observed to have the phase transition involved in the transformation from the NaCl-type to the CsCl-type structure under high pressure (3). A similar phase transition was confirmed even in NaCl (4). Among the alkali chlorides, no high-pressure transition was observed for LiCl. CsCl transforms from a NaCl-type structure to a CsCl type structure at 743 K and atmospheric pressure (5), the pressure required for the transition in RbCl is only several kbars, while for KCl and NaCl the pressure required should be above 15 kbars (5).

The Laplace pressure exerting on a small solid cluster may reach several kbars for alkali halides (6). Obviously, the Laplace pressure on a $(NaCl)_{108}$ cluster was not high enough to reach the transition required level; only the NaCl-type structure was observed in our previous study on $(NaCl)_{108}$ (7). RbCl is an interesting candidate for the phase transition from the liquid to the solid and possibly the transition from solid to solid due to its required pressure, for the solid–solid transition is near the Laplace pressure level for a small cluster. The study on the liquid to solid transition will provide the interfacial free energy information between the liquid and the solid, which will allow us to estimate the Laplace pressure on the small solid cluster and to explain the possibility of the transition from a NaCl-type solid to a CsCl-type solid. In this paper we report our MD simulations on $(RbCl)_{108}$ clusters.

EXPERIMENTAL PROCEDURE OF COMPUTATION

The MD simulations were performed on the clusters by using a modified version of the program MDIONS (8) in which the leapfrog algorithm was used to propagate the system's evolution. Configuration energies of a rock salt ionic cluster considerably depend on its shape. From our calculation the cubic-shaped rock salt ionic cluster has the lowest configuration energy, and therefore we chose the cubic-shaped cluster as the starting point. The initial configuration was based on the face-centered cubic cell with Rb^+ at (0, 0, 0), Cl^- at $(\frac{1}{2}, \frac{1}{2}, \frac{1}{2})$, and cell dimension of 6.581 Å, which was determined at 300 K (9). 108 Rb^+ and 108 Cl^-

[1] To whom correspondence should be addressed.

0022-4596/01 $35.00

TABLE 1
Potential Parameters for RbCl Used in the Simulation

	Rb^+–Rb^+	Rb^+–Cl^-	Cl–Cl^-
A (J/molecule)	4.255×10^{-20}	3.380×10^{-20}	2.535×10^{-20}
σ (nm)	0.3174	0.3172	0.3170

ions were initially arranged in a cubic-shaped cluster with each edge length 3 times the unit cell. The interaction potential used was Born–Mayer–Huggins (10–13),

$$U = \Sigma\{q_i q_j r_{ij}^{-1} + A_{ij} \exp[(\sigma_{ij} - r_{ij})/\rho]\}, \qquad [1]$$

where the first term is a simple Coulomb interaction and the second is the short-range repulsive interaction caused from the overlap of the filled electronic shells of the ions. Here, q_i and q_j are the charges on the ions i and j and r_{ij} represents the distance between ions i and j. The values of constants A_{ij} and σ_{ij} are calculated from the parameters given by Tosi and Fumi (13) and are given in Table 1. The value of constant $\rho = 0.318$ Å for RbCl is taken from Tosi and Fumi (13).

To melt a cluster, the simulation was started with 5000 time steps in a bath at 298.15 K followed by 5000 additional time steps at constant energy and then 5000 time steps were repeated in a bath at 298.15 K followed by 10000 time steps at constant energy. A series of heating stages began at 320 K, each succeeding stage being 20 K warmer than the previous one. Each stage was first simulated at constant temperature for 5000 time steps followed by 5000 time steps at constant energy. Heating was continued up to 1000 K, which is 10 K above the melting point of the bulk.

Freezing was simulated in a manner similar to that used in the melting process. In the slow cooling process the melted clusters were cooled through a series of stages that started from 900 K, each succeeding stage being 20 K cooler than the previous one until the clusters reached 220 K. Such a process corresponds to a heating/cooling rate of 2.5×10^{11} K/s.

Because of the stochastic character of crystal nucleation, detailed nucleation rate analysis of crystallization from the liquid at each temperature was evaluated from 17 nucleation events starting from 17 completely melted systems with different thermal histories. These completely melted systems were generated by continuing the heating after a cluster was melted at 900 K to form 17 clusters, each with 2000 more time steps than the previous one. Nucleation was studied by directly quenching these completely melted clusters into heat baths with temperatures at 500, 550, and 600 K.

In all the simulations the time step was set at 8 fs. The temperature was controlled by rescaling the kinetic energy of the cluster to the bath temperature with fluctuation at most 5 K before rescaling was performed. No external pressure control was added to the system.

DIAGNOSIS

Various diagnostic tests were applied for the heating and cooling process to monitor the behavior of ions. Melting and freezing were ascertained by observing the temperature dependence of the caloric curve, the Lineman index δ, and the pair correlation function $g(r)$. The MACSPIN progra m offers a very convenient way to view the image of the arrangement of ions and to monitor the progress of a phase change. The criterion used in our previous studies[7] of $(NaCl)_{108}$ was employed to analyze the nucleation of crystallization of $(RbCl)_{108}$ clusters.

ESTIMATION OF NUCLEATION RATE AND INTERFACIAL FREE ENERGY

The details of how to estimate the nucleation rates from our MD simulation are given in Appendix A1. Appendix A2 gives the information related to the estimation of interfacial free energies and diffuse interface thickness from nucleation theories. Thermal properties for RbCl used in this estimation are given in Appendix A3.

RESULTS

I. Cluster Melting and Freezing

The most important step in studying the nucleation kinetics of freezing is to completely melt the cluster so that there is no potential nuclei, which can become an embryo of crystallization during the cooling process. All the diagnostic tests mentioned in the previous section are helpful in choosing such a starting point of cooling runs.

Figure 1 presents images of the cubic $(RbCl)_{108}$ cluster generated by the MACSPIN program at several stages during the heating and cooling processes. When an ordered crystalline cluster was heated at 320 K, small vibrations of the ions around their equilibrium positions can be seen in Fig. 1A. At higher temperature the amplitude of the vibration becomes larger, as shown in Fig. 1B (600 K). The melting started from the surface of the cluster when it was immersed into the heat bath at 880 K (Fig. 1C) and completed at the end of 70 ps at this temperature (Fig. 1D). When the melted cluster was heated at 920 K for 80 ps, one molecule evaporated (Fig. 1E, the evaporated molecule was removed in the figure). No spherical liquid droplets can be seen from Figs. 1D and 1E. As shown in Fig. 1F, the melted liquid $(RbCl)_{108}$ droplet can be supercooled down to 620 K at the cooling rate mentioned before, a supercooling of $\sim$260 K below the melting temperature of the cluster. Crystallization started near the surface (Fig. 1G) after the liquid droplet was cooled in the heat bath at 600 K for less than 8 ps. At the end of 80 ps in the 600 K bath (Fig. 1H) a crystal-like solid was formed. The crystal frozen from the melt in this process has a stepped surface, as shown in Figs. 1I

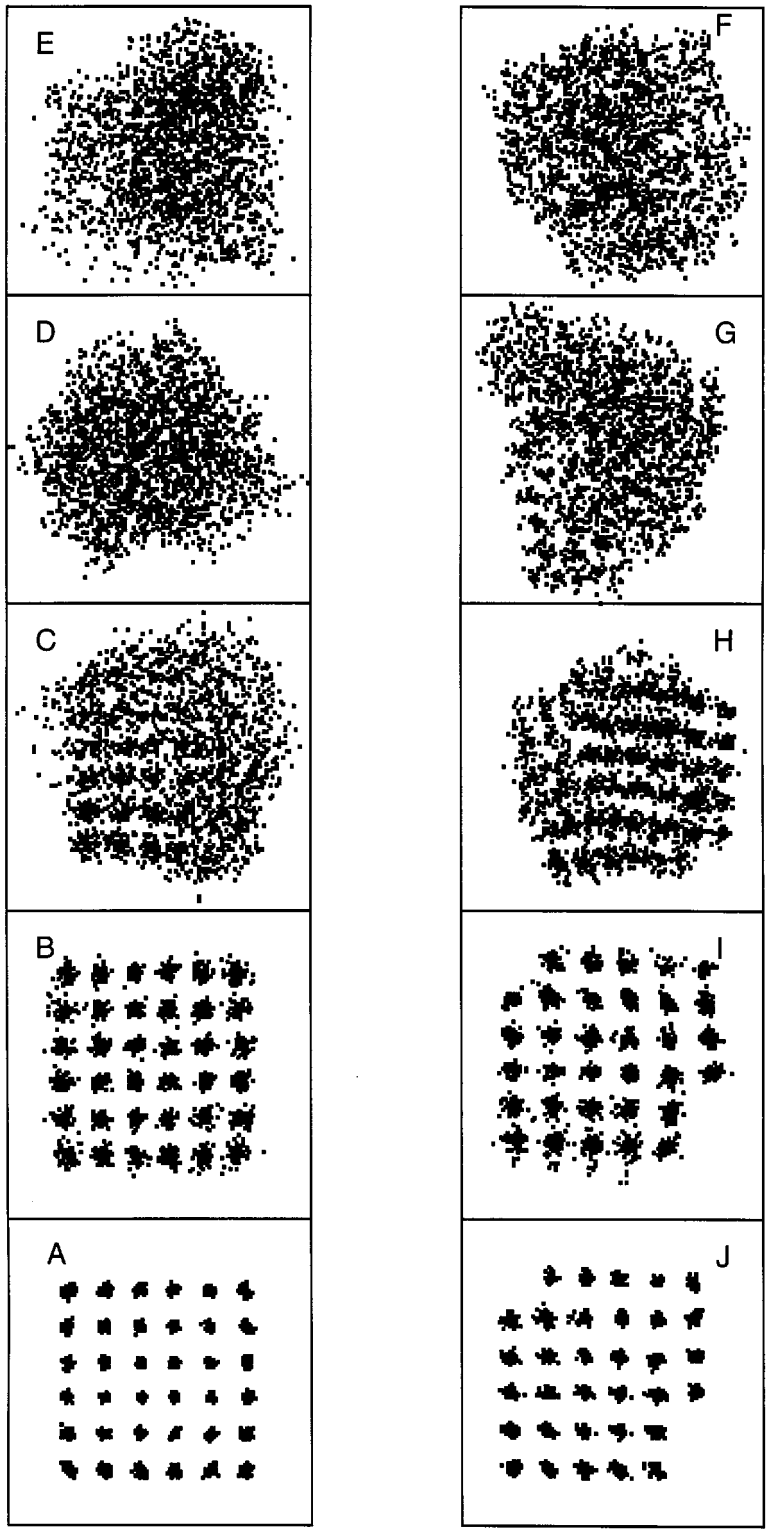

FIG. 1. Images of the $(RbCl)_{108}$ cluster at various stages of heating (left-hand column) and cooling (right-hand column). Temperatures of left-hand figures: (a) 320 K, (b) 600 K, (c) 10 ps in 880 K, (d) 70 ps in 880 K, and (e) 920 K. Right-hand figures: cooling from 920 K, (f) 620 K, (g) 8 ps at 600 K, (h) 80 ps at 600 K, (i) 560 K, and (j) 340 K.

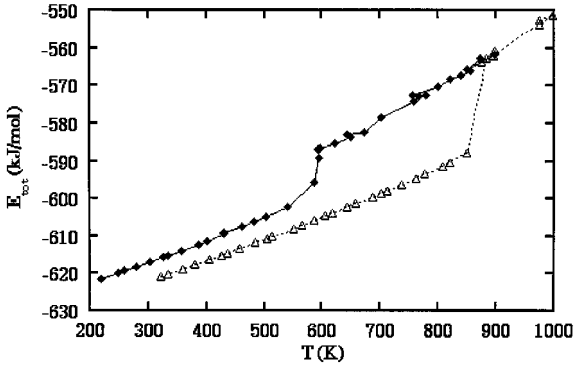

FIG. 2. Total energy per mole of the $(RbCl)_{108}$ cluster as a function of temperature during the heating (dotted curve) and cooling (solid curve) stages.

and 1J. It is clear from Figs. 1A and 1J, the packing of the crystal before the melting and after the crystallization are the same, FCC NaCl type crystal was crystallized from this cooling process.

The phase changes are readily recognized in the total energies of the cluster as a function of temperature given in Fig. 2. We prefer to use the midpoint of a jump in the total energy curve for the heating run as the melting temperature of a cluster. According to this definition the $(RbCl)_{108}$ cluster melted at 880 K, which is consistent with the information obtained from the images given in Fig. 1. The cooling curve usually is unsatisfactory for a similar definition because the stochastic nature of the nucleation initiating a phase change makes the temperature unpredictable and irreproducible; therefore, we prefer to use the bath temperature in the cooling run, in which the crystallization started, as the freezing temperature. It is located at ~ 600 K. Such a freezing temperature does not have any significance; we only used this as a reference to choose the temperatures for nucleation studies. Above this temperature we found it difficult to crystallize a molten cluster within a proper period of time. Therefore, the nucleation temperatures we chose were at 600 K and below for this study.

Pair correlation functions for Rb–Cl were calculated at different heating and cooling stages. Selected results of the calculations are shown in Fig. 3. Figures 3b (heating at 860 K) and 3c (heating at 900 K) clearly show the feature of pair correlation functions of the solid to the liquid and therefore the melting was located between these two points, i.e., the heating in the bath at 880 K. During the cooling process the pair correlation curve at 620 K maintains the liquid feature (Fig. 3d), while long range ordering features appear from the 580 K bath. The crystallization occurred at 600 K can be estimated under the aforementioned cooling rate.

The Lindemann index, $\delta(t)$, is the microscopic quantity commonly used to locate the melting transitions. It was

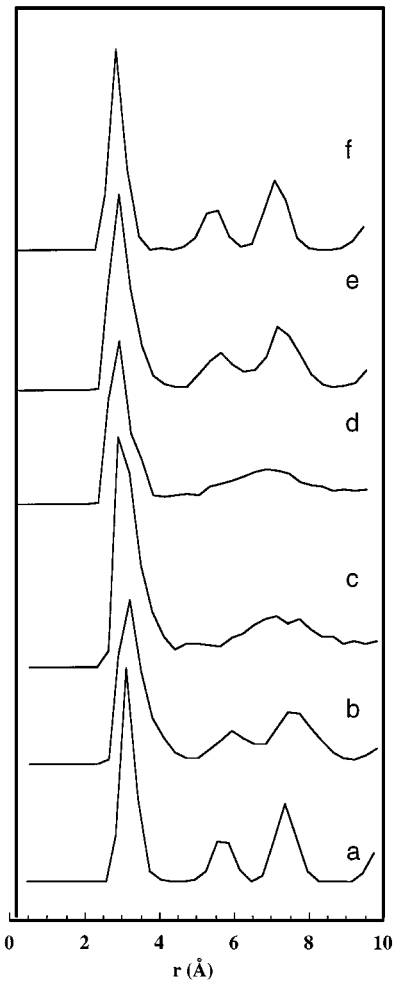

FIG. 3. Pair-correlation functions for Rb^+ and Cl^- ions in $a(RbCl)_{108}$ cluster at various temperatures during the heating and cooling stages. From bottom to top, heating (320, 860, and 900 K) and cooling (620, 580, and 340 K).

calculated from the ratio of the root-mean-square amplitude of vibration between adjacent particles to the mean distances between them. The criterion used for clusters of Lennard-Jones atomic clusters is that when $\delta(t)$ exceeds 0.1 the clusters are generally considered melted, for clusters of polyatomic molecules the melting was set to a smaller $\delta(t)$ value, and for ionic clusters the standard was also found to be lower than 0.1 (7). Figure 4 plots the Lindemann index, $\delta(t)$, for the heating and slow cooling processes based on the cutoff distance of 5.5 Å. It is clear that the exact value of $\delta(t)$ is not so important in the present system; the sharp change of this index is good enough to locate the melting and freezing transitions. The melting and crystallization temperatures located from the sharp changes in $\delta(t)$ are consistent with those obtained from the caloric curves. The $\delta(t)$ value at the starting point of the sharp change is lower than 0.1 in this case.

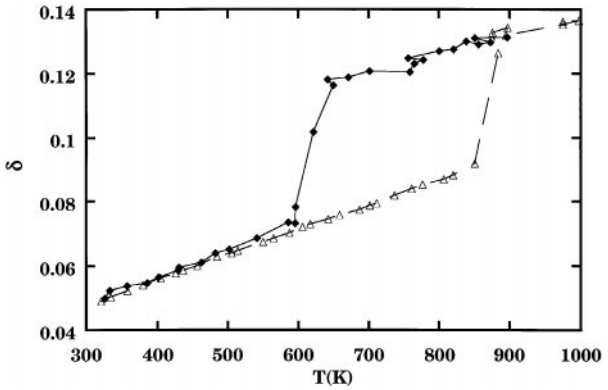

FIG. 4. Lindemann index $\delta(T)$ averaged over all Rb^+Cl^- ionic pairs in a $(RbCl)_{108}$ cluster as a function of temperature during stages of heating (triangles) and cooling (solid squares).

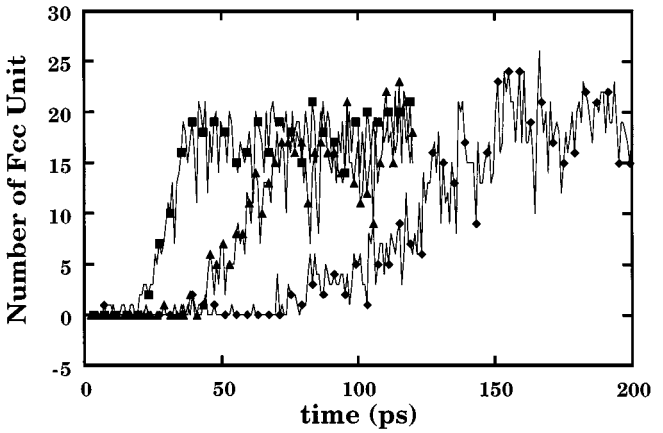

FIG. 6. Number of modified Voroni polyhedra as a function of time during the quench runs. Solid squares, quenched to 500 K bath; solid triangles, quenched to 550 K bath; solid rhombus, quenched to 600 K bath.

Based on these diagnoses, it is clear that when the cubic-shaped cluster constructed from 108 Rb^+ and 108 Cl^- was heated from the FCC phase at the heating rate mentioned before, it melted at around 880 K. When it was heated to 920 K, Rb^+ and Cl^- ions evaporated. To start from completely melted cluster but without losing any ions because of the evaporation, the cluster melted at 900 K was chosen as the starting point of the cooling. There are no potential nuclei for freezing left in the melt based on the criterion described in our previous paper (7).

II. Crystal Nucleation

Among the 17 quenching runs from 900 to 600 K, 16 systems resulted in a NaCl-type crystalline phase at the end of 720 ps. All 34 quenching runs to 550 and 500 K crystallized into NaCl-type crystals within 240 ps.

As shown in Appendix A1, the nucleation rate of the crystallization can be estimated from time t and the effective nucleation volume V_e.

The information about time t, the time at which a critical nucleus appears, can be estimated from the number of polyhedra that satisfy our criterion. Figure 6 shows the typical examples of time evolution of the number of qualified polyhedra for the $(RbCl)_{108}$ cluster during the quenching in the heat bath at 600, 550, and 500 K. The t value was usually identified as the time step at which the instantaneous configuration energy began a concerted descent toward the new phase (14), as shown in Fig. 5, while the t_0 value was usually set at the time of entry into the heat bath (14). It is more obvious to identify the t value from Fig. 6 because the starting point of growth of the FCC phase is clearly shown on the curves plotted in this figure. Table 2 lists the N/N_0 values as a function of time identified from the 50 curves similar to those plotted in Fig. 6. The

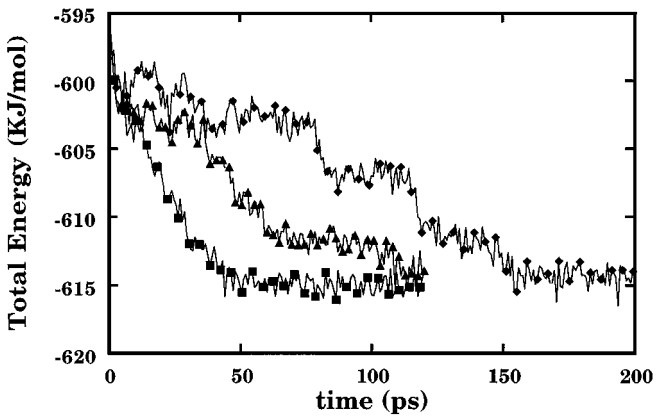

FIG. 5. Configuration energy as a function of time during the quenching. Solid squares, quenched to 500 K bath; solid triangles, quenched to 550 K bath; solid rhombus, quenched to 600 K bath.

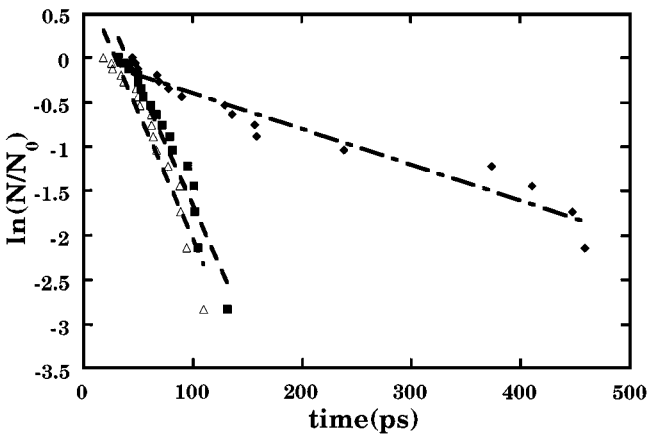

FIG. 7. $\ln[N/N_0]$ vs time plot from 50 MD quenching runs.

TABLE 2
Freezing Times and Temperatures of 50 Quenching Runs

500 K		550 K		600 K		
Run no.	t (ps)	Run no.	t (ps)	Run no.	t (ps)	N/N_0
5	19.2	1	32.8	9	45.6	1
8	26.4	17	37.6	3	48.0	16/17
17	27.2	15	42.4	16	50.4	15/17
15	35.2	2	50.4	17	68.0	14/17
11	37.6	4	50.4	2	69.6	13/17
4	48.8	14	52.8	11	78.4	12/17
6	50.4	9	55.2	7	90.4	11/17
16	52.0	3	61.6	10	129.6	10/17
9	62.4	16	67.2	15	136.0	9/17
12	62.4	7	72.0	13	156.8	8/17
14	64.0	6	79.2	1	158.4	7/17
10	67.2	11	81.6	8	238.4	6/17
13	77.6	13	95.2	14	373.6	5/17
3	88.0	10	100.8	6	410.4	4/17
2	88.8	12	101.6	12	447.2	3/17
7	94.4	5	104.8	5	458.4	2/17
1	109.6	8	131.2	4	*	1/17

plots with the $\ln[N/N_0]$ vs time obtained from 50 runs at three different temperatures are given in Fig. 7.

The total volume of the cluster was used as the effective volume for the nucleation. The nucleation rates estimated based on these t and V_e values are $\sim 3.75 \times 10^{36}$, 3.62×10^{36}, and $7.27.1 \times 10^{35}\ m^{-3}\,s^{-1}$ at temperatures of 500, 550, and 600 K, respectively.

DISCUSSION

I. Temperature Dependence of Interfacial Free Energy

As described in Appendix A2, interfacial free energy between the solid and the liquid, σ_{sl}, can be derived from the nucleation rate obtained from our simulation via the combinations of various prefactors with the exponential part from these theories. The estimated interfacial free energies and the diffuse interfacial thickness from different theories at different temperatures are given in Table 3. The interfacial free energy estimated from the classical nucleation theory (CNT) increases with increasing the temperature; however, it is contrary to the direction from the Grant–Gunton (GG) theory.

Usually, the interfacial free energy was thought to increase with increasing temperature; therefore, we prefer to use the results from CNT. The temperature dependence of σ_{sl} has been taken as the following empirical form (15)

$$\sigma_{sl}(T) = \sigma_{sl}(T1)(T/T1)^n, \qquad [2]$$

where n is a number presumably much smaller than unity. A value between $n = 0.3$ and $n = 0.4$ was obtained from the freezing experiment of mercury (15), it is reasonable to relate the interfacial free energies of water (16) obtained at ~ 195 and ~ 240 K by using $\sigma_{sl}(T) \sim \sigma_{sl}(T1)(T/T1)^{0.3}$. If a similar formula is used for the present case, the n value is around 1.1 in the temperature range of 500 to 600 K. This value is no longer smaller than unity. Whether the n value should be smaller than unity for any system remains to be investigated.

TABLE 3
Interfacial Free Energy/Interface Thickness Derived from Different Nucleation Theories

	500 K	550 K	600 K
	Interfacial Free Energy (mJ/m^2)		
CNT	39.0	41.5	48.0
G–G	73.5	70.5	67.0
	Interface Thickness (Å)		
DIT	1.95	1.88	2.01

One possible reference interfacial free energy value can be obtained from Turnbull's empirical rule (17) that relates solid–liquid interfacial free energy to the heat of fusion per unit area at melting, i.e.,

$$\sigma_{sl} = k_t \Delta H_{fus}/(V_2 N_A)^{1/3}, \qquad [3]$$

where ΔH_{fus} and V represent the molar heat of fusion and molar volume and N_A is Avogadro's number. The k_t value of ~ 0.32 for metalloids and nonmetals and ~ 0.45 for metals has been used. To meet the estimated σ_{sl} value of $79.0\ mJ/m^2$ at the normal melting point of RbCl(990 K) from Eq. [2], a k_t value of 0.57 in Eq. [3] should be used. This k_t value seems much larger than those used in the mentioned systems.

II. Striking Feature of Ionic Alkali Halides

MD simulations have been widely used in the nucleation of monoatomic and polyatomic molecular systems. In our previous paper we reported the MD studies in the ionically bonded $(NaCl)_{108}$ system. It is interesting to compare the results of ionic alkali halides with other systems.

One of the obstructions in current nucleation study of MD simulation is the computer speed that restricts most of the simulation work performed within a short period of time. Because of this limitation, only very few studies of nucleation of crystallization have been reported. One striking feature for $(RbCl)_{108}$ and $(NaCl)_{108}$ is that they are able to crystallize into crystals from their molten droplets even at an unrealistically fast cooling rate such as in the case of quenching them into a bath at a temperature much lower than their melting points. This feature makes it possible for us to perform systematic nucleation studies on this system.

Results on other alkali halides will be reported in forthcoming papers.

The potential functions for alkali halides have been studied for many years. In one of our recent studies, we realized that these potential functions are very reasonable for estimating the properties of small alkaline halides clusters (6). We believe the nucleation results based on these potential fields are meaningful.

III. Transition from NaCl-Type to CsCl-Type Structures

Our MD simulations on small NaCl and RbCl clusters did not show any phase transitions from a NaCl-type solid to CsCl-type solid, though we expected high Laplace pressure acting on small clusters. A rough estimation may explain the result.

The observation of the solid–solid phase transition in alkali halides depends on two factors. First, the pressure on the cluster has to reach the required value for such a transition. Second, the rate of such a transition must be within the limitation of the current simulation time period.

For a cubic cluster, the Laplace pressure is

$$P_{\mathrm{L}} = 4\sigma_{\mathrm{sv}}/L, \qquad [4]$$

where L is the edge length of the cubic cluster. From Youngs' equation we have

$$\sigma_{\mathrm{sv}} = \sigma_{\mathrm{lv}} + \sigma_{\mathrm{sv}}\cos(\theta), \qquad [5]$$

where θ is the contact angle. If we use the σ_{lv} value of 0.117 J/m^2 estimated from the formula given in Table A3 at 400 K, the σ_{sl} value of 0.04 J/m^2 estimated from Eq. [2], the maximum $\cos(\theta)$ value of 1, and the edge length of the $(\mathrm{RbCl})_{108}$ cluster, the obtained maximum Laplace pressure acting on the cluster is about 2.3 kbar. This high pressure is still below the phase transition required pressure of 5.2 kbar [5]. If the salt is really not wetted by its liquid, the Laplace pressure is even lower. Therefore, no transition from NaCl-type to CsCl-type structure for $(\mathrm{RbCl})_{108}$ will be expected from these data.

It is possible to reduce the size of the clusters to increase the Laplace pressure on the cluster. From Eq. [4] we have to reduce the edge length of the cluster to ca. one-third of its current size to reach the required pressure for the solid–solid phase transition if the molten liquid completely wets its solid and to one-fifth if it does not. Simulations on such a small cluster may not be meaningful for the phase transition studies.

CONCLUDING REMARKS

The freezing of supercooled liquid clusters of $(\mathrm{RbCl})_{108}$ has been observed by MD simulation and the homogeneous nucleation rates were determined to be 7.27×10^{35}, 3.62×10^{36}, and $\sim3.75\times10^{36}$ m^{-3} s^{-1} at temperature of 600, 550, and 500 K, respectively. From the measured nucleation rates, we obtained the values of 48.0, 41.5, and 39.0 mJ/m^2 of solid–liquid interfacial free energies at these temperatures. The Laplace pressure acting on the cluster is not high enough for the solid–solid phase transition to occur in a $(\mathrm{RbCl})_{108}$ cluster.

APPENDIX A1

Estimation of Nucleation Rate

Based on the assumption that the fraction of unfrozen clusters obeys the first-order rate law,

$$N_n(t_n)/N_0 = \exp[-JV_{\mathrm{e}}(t_n - t_0)], \qquad [A.1.1]$$

where N_0 is the total number of clusters, J is the nucleation rate, V_{e} is the effective volume in nucleation, t_{n} is the time at which the nth nucleation event in the set of N_0 clusters has taken place, t_0 is the time lag to achieve a steady state precritical nuclei, and N_n (t_n) is defined as (18)

$$N_n(t_n) = N_0 - n + \Delta, \qquad [A.1.2]$$

where the quantity Δ is taken as 1. Equation [A.1.2] can be written as

$$\ln[N_n(t_n)/N_0] = -JV_{\mathrm{e}}(t_n - t_0). \qquad [A.1.3]$$

Therefore, from the slope of the curve $\ln[N_n(t_n)/N_0] \sim t_n$ it is able to obtain J, the nucleation rate of freezing.

APPENDIX A2

Estimation of Interfacial Free Energy

For a homogenous nucleation the rate can be expressed by (19, 20)

$$J(T) = A\exp(-\Delta G^*/k_{\mathrm{B}}T), \qquad [A.2.1]$$

where k_{B} is the Boltzman constant, T is the temperature, and ΔG^* is the free energy barrier to the formation of a critical nuclei from the liquid.

For the classical nucleation theory (here after CNT) ΔG^* for a spherical nuclei is given by

$$\Delta G^* = 16\pi\sigma_{\mathrm{sl}}^3/[3(\Delta G_{\mathrm{v}} + w')^2], \qquad [A.2.2]$$

in which σ_{sl} is the interfacial free energy between the solid and liquid, ΔG_{v} represents the free energy of freezing per unit volume, and w' the work per unit volume of changing

the surface area of the liquid phase during the formation of the nucleus, which is expressed as

$$w' = P_L(\rho_l - \rho_s)/\rho_l, \qquad [A.2.3]$$

where P_L is the Laplace pressure $2\sigma_l/r_0$ inside the cluster and ρ's are densities of the liquid and solid.

The free energy of freezing per unit volume, $\Delta G_v(T)$, in Eq. [A.2.2] can be estimated from the standard thermodynamics

$$\Delta G_v(T) = (1/V)\int_{T_m}^{T} \Delta S_{fus}(T)\, dT, \qquad [A.2.4]$$

where V is the molar volume, $\Delta S_{fus}(T)$ is the molar entropy change of fusion at temperature T and it can be calculated by extrapolating the difference between the heat capacities of the liquid and solid. The heat capacity difference between the solid and the liquid in this study was estimated from our MD simulations; the result is given in Table A1.

In the diffuse–interface theory (DIT) (21–24) ΔG^* is given by

$$\Delta G^* = -4\pi\delta^3\Delta G_v\psi/3, \qquad [A.2.4]$$

where δ is the thickness of the diffuse interface and ψ is defined as (18)

$$\psi = [2(1+Q)H^{-2} - (3+2Q)H^{-1} + 1]/\eta, \quad [A.2.5]$$

with $\eta = \Delta G_{fus}/\Delta H_{fus}$, $H = \eta(1+\zeta)$ with $\zeta = w'/\Delta G_v$, and $Q = (1-H)^{1/2}$.

Both CNT's and Grant-Gunton's (GG) (25) prefactors were tested. The conventional formula for CNT's prefactor used is

$$A_{cl} = 16(\tfrac{3}{4}\pi)^{1/3}(\sigma_{sl}/k_BT)^{1/2}D/v_m^{2/3}\Delta r^2, \qquad [A.2.6]$$

TABLE A1
Physical Properties of RbCl Used in the Calculation

Property	Value or expression	Ref.
T_m (K)	990	CRC handbook
T_b (K)	1663	CRC handbook
ΔH_{fus} (J/mol)	18409	CRChandbook
C_p (l) $- C_p$ (s) (J/mol K)	$-4.48 + 0.0154T$	This work
V_m (solid) (m^3/mol)	4.32×10^{-5}	CRC handbook
V_m (liquid) (m^3/mol)	5.79×10^{-5}	CRC handbook
λ_1 ($wm^{-1}K^{-1}$)	$0.269 + 0.0009T$ (K)	30
D (Rb^+) (m^2/s)	$2.51\times10^{-7}\exp(-4031/T)$	31
D (Cl^-) (m^2/s)	$1.67\times10^{-7}\exp(-3734/T)$	31
D (RbCl) (m^2/s)	$2.09\times10^{-7}\exp(-3883/T)$	This work
ξ (Å)	$2.2\times10^{-10}(T/T_m)^{1.3}$	27–29
σ_{vl} (J/m^2)	$0.1450–6.979\times10^{-5}T$	32

where D is the coefficient of diffusion in the liquid, v_m is the volume of a molecule in the solid, and Δr is the molecular jumper distance from the liquid to the solid taken to be $v_m^{1/3}$.

A modified CNT prefactor in DIT theory was used and it will be known as the DIT prefactor from now on. Its expression is

$$A_{DIT} = \rho_1 O\Gamma Z \qquad [A.2.7]$$

with $\rho_1 = 1/v_m$, $O = 4[4\pi R_s^{*3}/(3v_m)]^{2/3}$, $\Gamma = 6D\lambda^{-2}$, and $Z = [v_m/(2\pi R_s^{*2})][-\Delta G_0(R_s^* - \delta/H)/(k_BT)]^{1/2}$; here, R_s^* is the radius of the nuclei which is calculated from $R_s^* = \delta(1+Q)H^{-1}$, λ is the jump distance in the liquid phase, and ΔG_0 is the free energy difference per molecule between the supercooled liquid and the solid.

The GG prefactor can be expressed as (26)

$$A_{GG} = 1.54\lambda_1(\sigma_{sl})^{7/2}/[(k_B)^{3/2}T^{1/2}L^2(-\Delta G_v)\xi^4], \qquad [A.2.8]$$

where λ_1, L, and ξ represent the thermal conductivity, heat of fusion per unit volume of solid, and a correlation length characterizing the thickness of the interface between the solid and liquid. The temperature dependence of ξ was estimated from the results of Refs. (27–29).

APPENDIX A3
Physical Properties of RbCl Used in the Calculation

Physical properties needed for the calculation of interfacial free energy are summarized in Table A1.

ACKNOWLEDGMENTS

This work was supported by a grant from Nanjing Normal University of P. R. China and a grant from the National Science Foundation of The United States to the University of Michigan.

REFERENCES

1. J. C. Slater, *Phys. Rev.* **23,** 488 (1924).
2. R. B. Jacobs, *Phys. Rev.* **54,** 468 (1938).
3. P. W. Bridgman, *Z. Kristallogr.* **67,** 363 (1928); *Phys. Rev.* **48,** 893 (1935).
4. V. V. Evdokimova and Vereshchagin, *Sov. Phys. Sol. State* **4,** 1438 (1962/3).
5. C. W. F. T. Pistorius, *J. Phys. Chem. Solids* **25,** 477 (164).
6. J. Huang and L. S. Bartell, *J. Mol. Struc.*, in press.
7. J. Huang, X. Zhu, and L. S. Bartell, *J. Phys. Chem.* **102,** 2708 (1998).
8. N. Anastasiou and D. Fincham, "Program MDIONS," CCP5 Program Library, SERC Daresbury Laboratory, Daresbury, UK.
9. Swanson *et al. NBS Circular* **539 IV,** 41 (1953).
10. B. Born and J. E. Mayer, *Z. Phys.* **75,** 1 (1932).
11. M. L. Huggins and J. E. Mayer, *J. Chem. Phys.* **1,** 643 (1933).
12. M. L. Huggins, *J. Chem. Phys.* **5,** 643 (1937).
13. M. P. Tosi and F. Fumi, *J. Phys. Chem. Solids* **25,** 45 (1964).

14. K. Kinney, S. Xu, and L. S. Bartell, *J. Phys. Chem.* **100,** 6935 (1999).
15. J. Huang and L. S. Bartell, *J. Phys. Chem.* **99,** 3924 (1995).
16. G. M. Rothberg, M. Eisenstadt, and P. Kusch, *J. Chem. Phys.* **30,** 517 (1959).
17. D. Turnbull, *J. Appl. Phys.* **21,** 1022 (1950).
18. Y. Chushak, P. Santikary, and L. S. Bartell, *J. Phys. Chem.* **103,** 197 (1999).
19. D. Turnbull and J. C. Fisher, *J. Chem. Phys.* **17,** 71 (1949).
20. E. R. Buckle, *Proc. R. Soc. London A* **261,** 189 (1961); **261,** 197 (1961).
21. L. Granasy, *Europhys. Lett.* **24,** 121 (1993).
22. L. Granasy, *J. Non-Cryst. Solids* **162,** 301 (1993).
23. L. Granasy, *Mater. Sci. Eng. A* **178,** 121 (1994).
24. L. Granasy, *J. Phys. Chem.* **99,** 14183 (1995).
25. M. Grant and J. D. Gunton, *Phys. Rev. B* **32,** 7299 (1985).
26. J. Huang, W. Lu, and L. S. Bartell, *J. Phys. Chem.* **100,** 14276 (1996).
27. P. Harrowell and D. W. Oxtoby, *J. Chem. Phys.* **80,** 1639 (1984).
28. Y. C. Shen and D. W. Oxtoby, *J. Chem. Phys.* **104,** 4233 (1996).
29. Y. C. Shen and D. W. Oxtoby, *J. Chem. Phys.* **105,** 6517 (1996).
30. M. V. Smirnov, V. A. Khokhlov, and E. S. Filatov, *Electrochim. Acta* **32,** 1019 (1987).
31. G. W. Hooper, *Discuss Faraday Soc.* **32,** 218 (1961).
32. "International Critical Tables of Numerical Data, Physics, Chemistry, and Technology." McGraw-Hill, New York, 1926–1939.